Journal of Alloys and Compounds 509 (2011) 7702–7709

Contents lists available at ScienceDirect

Journal of Alloys and Compounds

journal homepage: www.elsevier.com/locate/jallcom

Synthesis and characterization of Pt–Pd nanoparticles with core-shell morphology: Nucleation and overgrowth of the Pd shells on the as-prepared and defined Pt seeds

Nguyen Viet Long[a,b,c,d,*], Tong Duy Hien[c], Toru Asaka[a], Michitaka Ohtaki[d], Masayuki Nogami[a,**]

[a] Department of Materials Scienceand Engineering, Nagoya Institute of Technology, Gokiso-cho, Showa-ku, Nagoya 466-8555, Japan
[b] Posts and Telecommunications Institute of Technology, km 10 Nguyen Trai, Hanoi, Viet Nam
[c] Laboratory for Nanotechnology, Vietnam National University at Ho Chi Minh, Linh Trung, Thu Duc, Ho Chi Minh, Viet Nam
[d] Department of Molecular and Material Sciences, Interdisciplinary Graduate School of Engineering Sciences, 6-1 Kasugakouen, Kasuga, Fukuoka 861-8580, Japan

ARTICLE INFO

Article history:
Received 29 November 2010
Received in revised form 5 April 2011
Accepted 5 April 2011
Available online 27 April 2011

Keywords:
Pt–Pd core-shell nanoparticles
The as-prepared and defined Pt cores
The Pd shells
Polyol method
$AgNO_3$

ABSTRACT

In the present research, Pt–Pd core-shell nanoparticles based on the as-prepared and defined Pt-seed cores with well-controlled size and morphology were synthesized. Their characterizations were investigated by using UV–vis spectroscopy, transmission electron microscopy (TEM), and high resolution (HR)TEM measurements. The high resolution elemental mappings were performed in the operation of high angle annular dark field (HAADF) in conjunction with scanning (S)TEM mode and X-ray energy dispersive spectroscopy (XEDS). It is found that not only the Pt–Pd core-shell nanoparticles were formed, but also the nucleation, growth, and the separate formation of single Pd nanoparticles as well. Interestingly, the as-prepared Pt cores without the morphological changes were protected by the overgrowths of the Pd shells during the successive reduction of sodium tetrachloropalladate (II) hydrate. There were the co-existence of the Frank–van der Merwe (FM) layer-by-layer and Stranski–Krastanov (SK) island-on-wetting-layer growth modes of the Pd shells on the as-prepared Pt cores. It is predicted that the SK growth became the favorable growth mode in the formation of the Pd shells in the formation Pt–Pd core-shell nanoparticles.

1. Introduction

At present, Pt nanoparticles-catalysts are very interest because of their applications in catalysis and biology [1–4]. Moreover, their catalytic and electrocatalytic critical properties are tuned by controlling in both the size and the morphology. It is known that the morphologies of {1 1 1}, {1 0 0}, and {1 1 0} low-index planes or facets of Pt nanoparticles are very important in the selective catalytic reactions [5–8]. The general methods of chemically synthesizing Pt nanoparticles are utilized in a bottom-up approach in the reduction of their salts with suitable reducing agents and stabilizers, such as K_2PtCl_4 (potassium plantinum(II) chloride) [9,10], Na_2PtCl_4 (sodium tetrachloroplatinate(II) hydrate) [3], H_2PtCl_6 (dihyrogen hexachroplatinate(IV) hexahydrate), $Pt(acac)_2$ (platinum(II) acetylacetonate), and their ligands [3,11]. In order to improve their catalytic performance, new Pt-nanoparticles catalysts are developed [12]. Because of pure Pt-based catalyst of high cost, various kinds of Pt-based alloy and core-shell catalysts, ternary Pt-based catalysts, and even more various compositions have been developed and tested in proton exchange membrane fuel cells (PEMFCs) [3,12,38–55].

The core-shell structure is an excellent method of reducing the Pt-loading catalyst. Therefore, the Pd-shell case is studied to enable the effective-cost design. However, their un-controllable changes of the structures of the core and the shell occurred and remained. Accordingly, the electrochemical synthesis of core-shell catalysts for electrocatalytic applications were proposed and reported. The core-shell structure was not homogeneous or inhomogeneous structure [13]. Recently, Pt–Pd core-shell catalysts have demonstrated their enhanced electrocatalytic activity towards oxygen reduction reactions (ORR) and methanol oxidation reactions (MOR) [14]. Their catalytic and electrocatalytic characterizations are much better than Pt nanoparticles because of a synergetic property between the layers of the core, the shell, and their contact in the bifunctional core-shell configuration, high surface-to-volume ratio and quantum size as well. In particular, the synthesis of Pt–Pd nanoparticles by polyol method was considered [15,16]. In contrast to the oxide-shell case, the metal-shell layer grew in the uncontrollable and random modes on the metal cores. It was discovered

* Corresponding author at: Department of Materials Science and Engineering, Nagoya Institute of Technology, Gokiso-cho, Showa-ku, Nagoya 466-8555, Japan.
** Corresponding author.
E-mail addresses: nguyenvietlong@yahoo.com (N.V. Long), nogami@nitech.ac.jp (M. Nogami).

0925-8388/$ – see front matter © 2011 Elsevier B.V. All rights reserved.
doi:10.1016/j.jallcom.2011.04.031

that the epitaxial growth of a metal shell and in the non-epitaxial growth of an oxide shell were observed in the core-shell nanoparticles [17,18]. Thus, the overgrowth of the shell layer on the core with a lattice match and mismatch requires further clarification. The fabrication procedures of core-shell shaped bimetallic nanoparticles via a bottoms-up approach lead to the increasing complexity because of alloying and large lattice mismatches occurring between the core and the shell of two different metals. Moreover, the common alloying and surface phenomena of the core and/or shell are observed [19–28]. Therefore, the stability of core-shell configuration is necessarily achieved in the core, the shell, and their interfaces. Many researchers propose the combination of controlling strategies (chemical and physical methods and experimental conditions) and on the selection of metal precursors, reducing agents, and controlling reagents in the procedures of designing a practical core-shell bimetallic particle system [22–28]. Currently, Pd–Pt core-shell nanoparticles of the spherical porous structure by adjusting the molar ratio of Pd and Pt precursors have been synthesized by a one-step microwave heating method [14]. In this paper, we presented on a facile controlled synthesis of as-prepared and defined Pt cores through a modified polyol method in the presence of silver nitrate as a modifying agent at 160 °C. First, Pt nanoparticles were prepared by polyol method with the addition of $AgNO_3$ in the reduction of H_2PtCl_6 by ethylene glycol (EG). Then, the as-prepared Pt nanoparticles were employed as the as-defined cores for the overgrowths of the Pd shells in the successive reduction of Na_2PdCl_4 by EG. In addition, the results of Pt–Pd core-shell nanoparticles are very fascinating because the good overgrowths of Pd shells protect the sharp morphologies of as-prepared polyhedral Pt cores from the external chemical changes.

2. Experimental

2.1. Chemicals and materials

Chemicals from Aldrich and Sigma–Aldrich were used in the experimental processes. They were polyvinylpyrrolidone (PVP, a stabilizer) (FW: 55,000), sodium tetrachloropalladate(II) hydrate (Na_2PdCl_4) (ACS reagent), and chloroplantinic acid hexahydrate (H_2PtCl_6) (ACS reagent) as precursors for producing Pd nanoparticles (Sample 1), Pt nanoparticles (Sample 2), Pd and Pt–Pd nanoparticles (Sample 3). Ethylene glycol (EG) was used as both the solvent and the reducing agent. Silver nitrate (metal basis) was used as a modifying agent. Solvents including ethanol, acetone, and hexane were used for washing and cleaning. Ionized, distilled, and mili-Q water were prepared using a Narnstead nanopure H_2O purification system. All chemicals used were of analytical grade and were used without any further purification.

2.2. Synthesis of Pd nanoparticles

Briefly, a volume containing 5 mL of EG was put in a volumetric flask, heated at 160 °C, and stirred for 1 h. Then, an amount of about 0.016 g of Na_2PdCl_4 was dissolved in 3 mL of EG at room temperature under stirring for 1 h. The color of mixture became typically red–brown and showed the existence of $[PdCl_4]^{-2}$ ions in EG. Then, an amount of 0.031 g of PVP was dissolved in 3 mL EG so that the molar ratio of PVP/Pd salt was ~12:1. The mixture of PVP and EG was stirred for 2 h. To synthesize Pt nanoparticles, the contents of the stock solutions of PVP and Pd precursors were directly injected into the flask. First, 60 μL of PVP was injected into the flask. After 30 s, 30 μL of Na_2PdCl_4 was rapidly added into the flask. The sequential injection of PVP and Na_2PdCl_4 precursors was repeated until their total volumes were thoroughly used. Then, the solution was kept in the flask under stirring for 5 min. The reduction of Na_2PdCl_4 by EG was occurred. Finally, Pd nanoparticles were formed in the stabilization of PVP and the extra EG solvent. The color of the product was dark-brown. To obtain the pure product, the procedures of washing and cleaning, removing PVP polymer from the product by the mixture of ethanol–hexane in the volume ratio of 1:3 were carried out and repeated until the pure Pd nanoparticles were dispersed in ethanol (Sample 1).

2.3. Synthesis of Pt nanoparticles

During the controlled synthesis of the Pt nanoparticles, 3 mL of EG, 1.5 mL of 0.0625 M H_2PtCl_6, 3 mL of 0.375 M PVP, and 0.5 mL of 0.04 M $AgNO_3$ were used. The volumes of 3 mL EG and 0.5 mL 0.04 M $AgNO_3$ were mixed in a flask and heated to 160 °C. After the solution was mixed for 15 min, argon gas was bubbled for 20 min to purge out the oxygen present in the flask prior to the synthesis. The solution was refluxed for 2 h in an Ar gas atmosphere and sealed to avoid air from entering the flask. Next, 30 μL of 0.0625 M H_2PtCl_6 was added to the flask at 160 °C, sequentially followed by the injection of 60 μL of 0.375 M PVP into the flask until their total volumes were added and reacted thoroughly under continuously stirring for 15 min (1.5 mL of 0.0625 M H_2PtCl_6 and 3 mL of 0.375 M PVP). The reduction of H_2PtCl_6 occurred because of the EG present. The resultant mixture was stirred in the flask at 160 °C for 15 min. As a result, a dark brown solution containing the as-prepared Pt nanoparticles exhibited their polyhedral morphology (Sample 2).

2.4. Synthesis of Pt–Pd core-shell nanoparticles from the as-prepared Pt seeds

At first, Pt nanoparticles were synthesized by the above stable and reliable procedure. Then, they were used as the as-prepared and defined cores for producing the Pt–Pd core-shell nanoparticles. In a similar manner, 3 mL of EG and 0.5 mL of 0.04 M $AgNO_3$ were added to a flask, and the mixture was refluxed at 160 °C for 15 min. Then, 30 μL of 0.0625 M Na_2PdCl_4 was added in the flask, sequentially followed by the addition of 60 μL of 0.375 M PVP to the flask until their total volumes reacted thoroughly (1.5 mL of 0.0625 M Na_2PdCl_4 and 3 mL of 0.375 M PVP). The successive reduction of Na_2PdCl_4 by EG was occurred under continuously stirring for 15 min. After that, the resultant mixture was kept in the flask while stirring it for 15 min. Next, the flask containing the product solution was moved from the hot oil bath. In this process, the formation of both Pd and Pt–Pd core-shell nanoparticles were observed in the final product (Sample 3).

2.5. Characterization

The volumes of the reaction mixture were collected and used in an appropriate time during the synthesis. They were investigated by UV–vis–NIR spectroscopy (Ubest 570 UV–vis–NIR spectrotometer) for the comparison of kinetics and mechanisms of the formation of Pd (Sample 1), Pt (Sample 2), Pd and Pt–Pd nanoparticles (Sample 3). Meanwhile, 3 mL of ethanol of Pt nanoparticles was set onto the pieces of special glass for the XRD measurement with a small area around 1 cm^2. The drops of ethanol of Pd, Pt, Pd and Pt–Pd nanoparticles were poured on glass and were dried at 80 °C and 100 °C for 6 h prior to use. In addition, these slides were treated with ethanol to remove any impurities. The X-ray diffraction patterns were recorded by a diffractometer (X'Pert-Phillips) operating at 45 kV/45 mA and using Cu-Kα radiation (1.54056 Å) and at room temperature.

To characterize the Pd (Sample 1), Pt (Sample 2), Pd and Pt–Pd core-shell nanoparticles (Sample 3), copper grids of Samples 1, 2, and 3 containing Pd, Pt and, Pd and Pt–Pd core-shell nanoparticles were stored and maintained under vacuum (1–10 Pa) by using a vacuum cabinet (JEOL-EM-DSC10E Film Vacuum Desiccator Cabinet) for 2 days prior to the TEM and HRTEM measurements. Then, the copper grids were treated again at the drying station (JEOL JDS-230F Drying Station) for 1 day. They were treated using an ion cleaner that employed the glow discharge in vacuum (1–10^2 Pa) to remove any contamination (Ion Cleaner JIC-410 JEOL). Next, the copper grids were maintained under conditions of very high vacuum (10^{-6}–10^{-7} Pa) in the transmission electron microscope (JEOL JEM-2100F or JEM-2010) overnight prior to the TEM and HRTEM measurements. The TEM and scanning TEM (STEM) images were obtained using a transmission electron microscope (JEOL JEM-2100F and JEM-2010) operated at 200 kV. In addition, the microscope (JEOL JEM-2100F) was equipped with an ultra-high resolution objective lens and a STEM system. The STEM system enabled high angle annular dark field (HAADF) imaging. Elemental analyses were performed using an X-ray energy dispersive spectrometer (XEDS) (JEOL JED-2300). High resolution elemental mappings were carried out involving in the combination of STEM and XEDS (STEM-XEDS method). For acquiring, visualizing, analyzing, and processing digital image data of Pd, Pt, Pd and Pt–Pd nanoparticles, DigitalMicrograph software (Gatan, Inc.) was used in our TEM and HRTEM studies.

3. Results and discussion

3.1. UV–vis spectra and XRD patterns of Pd, Pt, Pd and Pt–Pd nanoparticles

Fig. 1(a) shows the typical UV–vis absorption spectra of the samples of PVP-Pd (Sample 1), Pt (Sample 2), Pd and Pt–Pd nanoparticles (Sample 3) by using 3 mL of ethanol and 30 μL of the resultant solutions of PVP-Pd, Pt, Pd and Pt–Pd nanoparticles. The comparative method of studying was also carried out in the UV–vis absorption spectra of PVP, $AgNO_3$, Na_2PdCl_4, H_2PtCl_6, Na_2PdCl_4 and H_2PtCl_6 in EG, and the product of PVP-Pd (Sample 1), Pt (Sample 2), Pd and Pt–Pd nanoparticles (Sample 3) with $AgNO_3$. There were the strong peaks at the centered range ~283.70 nm due to the ligand-to-metal charge-transfer transition of both $[PtCl_6]^{-2}$ and $[PdCl_4]^{-2}$ ions, and various kinds of ions (Ag^+ ions), PVP polymer, clusters, nanoclusters, and nanocrystals in EG. However, the UV–vis spectrum of Na_2PdCl_4 in EG also showed the strong peak

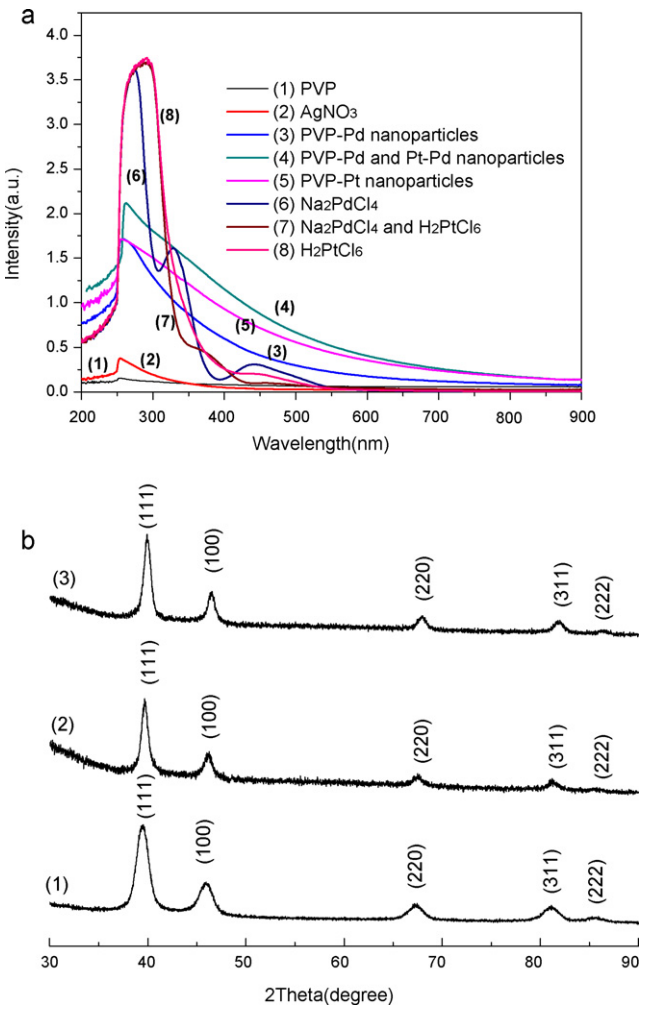

Fig. 1. (a) UV–vis spectra of PVP (1), $AgNO_3$ (2), PVP-Pd nanoparticles (S3), Pd and Pt–Pd nanoparticles (4), PVP-Pt nanoparticles (5), Na_2PdCl_4 (6), H_2PtCl_6 and Na_2PdCl_4 (7), and H_2PtCl_6 (8). (b) Three XRD patterns of various nanoparticles: (1) Pd and Pt–Pd core-shell nanoparticles, (2) Pt nanoparticles, and (3) Pd nanoparticles.

at 283.70 nm together with two specific peaks much weaker at 372.41 and 442.80 nm. In addition, the UV–vis spectra of both Na_2PdCl_4 and H_2PtCl_6 in EG showed the strong intensity of peaks at 282.85 nm and one peak much weaker at 446.32 nm.

The evidences were observed that the formation of Pd (Sample 1), Pt (Sample 2), Pd and Pt–Pd nanoparticles (Sample 3) stabilized by PVP was due to their considerable decreases in the absorption intensity. Clearly, the changes in UV–vis spectra showed the reductions of Pd and Pt ions, into metals, and their self-aggregation and assembly in the formation of Pd and Pt nanoparticles of final morphologies. It is proved that there was the sharp peak at ~283.70 nm attributed to the Ligand field splitting of Pt5d and Pd4d (or 5d) orbital expands and the coordination of N and/or O atoms of PVP to the surfaces of these nanoparticles [29]. The sample of only PVP polymer exhibited the very weak absorbance comparable to other samples of ions and nanoparticles. It was suggested that the initial seeds leading to clusters, and leading to that ultra-small size nanocrystals were formed in this process for a short time of 1–3 min, which related to their nucleation from ions into clusters and nanoclusters by their self-aggregation and assembly [30–33]. Then, the nucleation and growth processes happened simultaneously. Finally, the final product of PVP-Pd (Sample 1), Pt (Sample 2), Pd and Pt–Pd nanoparticles (Sample 3) were obtained in the extra EG solvent. These nanoparticles are stabilized by the layers or monolayers of PVP polymer because of the fact that PVP binds to the surface of the nanoparticles and sterically blocking them from contacting each other [30]. Therefore, PVP can bind to a metal surface through either the carbonyl or the tertiary amine of the pyrrolidone ring due to the covalent interactions at the surface.

Fig. 1(b) shows three typical XRD patterns of nanoparticles (Pd nanoparticles (Sample 1), Pt nanoparticles (Sample 2), Pd and Pt–Pd nanoparticles (Sample 3)). The results represent the property of their crystalline face centered cubic (fcc) phase. The XRD peaks of Pd (Sample 1), Pt (Sample 2), Pd and Pt–Pd nanoparticles (Sample 3) [33] were typically characterized by a system of (1 1 1), (2 0 0), (2 2 0), (3 1 1), and (2 2 2) specific XRD peaks in respective to the 2θ values of about 39.68°, 46.04°, 67.34°, 81.88°, and 85.93°, respectively. The XRD patterns of these nanoparticles are nearly similar in their appearance and shape. However, the intensities and the full widths at half maximum (FWHM) of the peaks were different. The XRD peaks of Pd (Sample 1), Pt (Sample 2), Pd and Pt–Pd nanoparticles (Sample 3) were broad and comparable to those of the corresponding bulk Pt crystal. One of the XRD peaks was adopted to determine the average size of their nanocrystallites on the basic of the width of the reflection according to the Debye–Scherrer equation: $D = 0.89\lambda/(\beta \cos\theta)$ [29,33], where β is the FWHM width of the peak, θ is the angle of diffraction, and λ is the wavelength of the X-ray radiation. Approximately, the (2 2 0) reflections of single-crystalline Pt nanoparticles are used to calculate the average size according to the above formula. The crystallite size of Pt particle was estimated ~8.20 nm in the XRD diagram in Fig. 1(b) (line (2)).

3.2. Size and morphology of Pd and Pt nanoparticles: role of $AgNO_3$

Fig. 2(a) shows the main kinds of various near-sphere and rod-like morphologies of Pd nanoparticles by modified polyol method at 160 °C for 15 min with the particle size of 7–16 nm (Sample 1). The Pd nanorods with the particle size around 12 nm and the twinned Pd nanoparticles were also observed. Therefore, the role of $AgNO_3$ in the morphological control of Pd nanoparticles was not clearly confirmed. Fig. 2(b) also shows TEM images of polyhedral Pt nanoparticles together with their truncated polyhedral morphologies with the particle size of 7–16 nm by modified polyol method at 160 °C for 15 min using PVP and the structure-controlling agent of 0.04 M $AgNO_3$ (Sample 2). Therefore, the assistance of $AgNO_3$ influenced on the final morphology and structure of Pt nanoparticles associated with their synthetic time. These sharp and polyhedral Pt nanoparticles of the characteristic low-index {1 0 0} and {1 1 1} facets are considered in their practical applications in catalysis [2–4]. Therefore, a modified polyol method using the assistance of $AgNO_3$ (or others inorganic chemicals) offers the good routes to synthesize metal nanoparticles under size and shape control [29]. For polyhedral Pt nanoparticles, it was observed that these Pt nanoparticles exhibiting the very good single-crystal structures were controlled in both the size and the morphology while non-polyhedral Pt nanoparticles were controlled in the size but they have the various morphologies in Fig. 3(a) because the reduction of H_2PtCl_4 by EG occurred for 35 min. In addition, various kinds of single and multiple twined Pd and Pt nanoparticles were also found in Fig. 3. The results indicated the polyhedral Pt nanoparticles in the homogenous single-crystal growth. There are two main kinds of the nucleation and growth of metal nanoparticles [3,31,34]. In our research, the homogeneous nucleation and growth become the preferential nucleation and growth. However, the heterogeneous nucleation and growth of Pt nanorod were observed in Fig. 3(a). The morphology of sphere-like non-polyhedral Pt nanoparticles needs to be studied in the further details, especially in their roles in catalysis. In fact, the morphologies of non-polyhedral Pt nanopar-

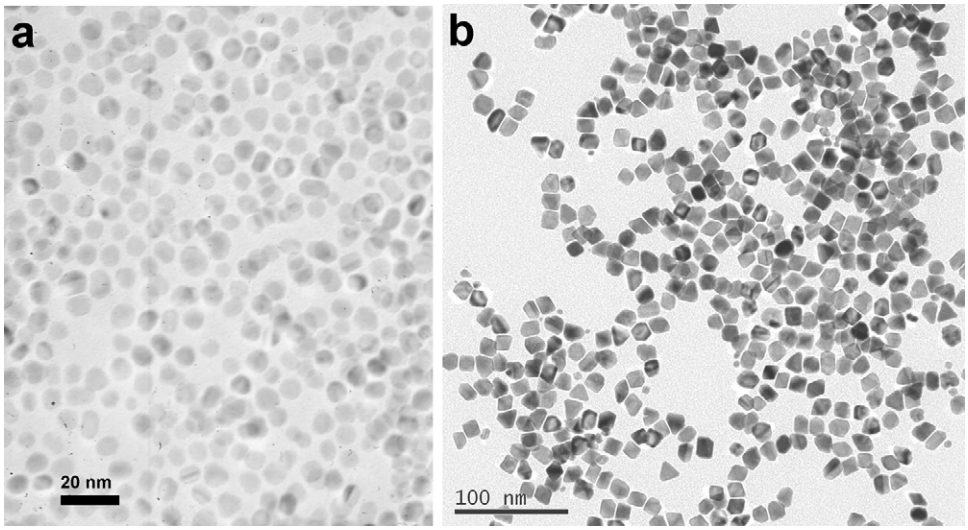

Fig. 2. TEM images: (a) Pd nanoparticles (Sample 1). (b) Pt nanoparticles by modified polyol method (Sample 2). Scale bars: (a) 20 nm; (b) 100 nm.

ticles are very complicated as shown in Fig. 3(a) and (e) both in the experimental TEM and HRTEM images and in their assumed models. The symmetry and regularity of the atomic arrangements on the external surface of octahedral Pt nanoparticle in Fig. 3(f) are better than that of sphere-like Pt nanoparticle in Fig. 3(e), which are illustrated in the models in Fig. 3(h) and (g). They are some of the good morphologies of well-controlled Pt nanoparticles. It was observed that the average particle size of polyhedral Pt nanoparticles was approximately 10 nm in the nanosized range of 7–16 nm in Fig. 3(b–d). Here the reduction of H_2PtCl_4 by EG occurred for 15 min. They are more than 90% of sharp and polyhedral Pt nanoparticles (three main kinds of cubic, octahedral, and tetrahedral Pt nanoparticles or various truncated cubic, octahedral, and tetrahedral Pt nanoparticles) indicating their very sharp corners, edges, and facets. An HRTEM image of a single Pt nanoparticle (Fig. 3(f)) shows the Pt lattice fringes with the inter-fringe distance ~0.230 nm close to the {1 1 1} planes showing Pt crystal of face-centered cubic (fcc) structure. However, the appearance of surface defects at the corners of polyhedral Pt nanoparticles. Therefore, they possess both the most characteristic low-index {1 0 0} and {1 1 1} planes in their polyhedral morphology. The surfaces of polyhedral Pt nanoparticles are the flat and sharp morphologies of better atomic arrangements in comparing with the un-flat surfaces of sphere-like and non-polyhedral Pt nanoparticles in the atomic arrangements. We proposed that the role of Ag^+ tends to direct the {1 0 0} and {1 1 1} selective growth modes of Pt nanoparticles leading to the formation of Pt nanoparticles with various polyhedral morphologies. However, the factors including the supply rates of polymer (PVP) and precursor (H_2PtCl_6), time and temperature are also very important to the appearance of polyhedral Pt nanoparticles instead of non-polyhedral Pt nanoparticles. It was known that the role of Ag^+ enhances the {1 0 0} growth, and/or suppresses {1 1 1} growth and Ag^+ is readily reduced by EG at high temperature resulting in reduced silver species, such as Ag_4^{2+} clusters and Ag^0 [29]. Thus, they are adsorbed on the surface of {1 0 0} facets and cations based on Pt nanoparticles. They are easily removed by organic solvents. Fig. 3(e) illustrates HRTEM images of non-polyhedral Pt nanoparticles with un-sharp shapes. They are different from with sharply polyhedral Pt nanoparticles but their fabrication in the near same experimental conditions. The illustrations of the formation of the terrace, ledge, and kinks of the particle surface were introduced, leading to form the positions of highly chemical reactivity due to their accessibility and coordinative un-saturation [7,8,35].

Typically, the non-polyhedral Pt nanoparticles have different shapes and morphologies in Fig. 3(a) without the sharp corners and edges as well as truncated corners as polyhedral Pt nanoparticles. In our observation, Fig. 3(a) shows the polyhedral and sphere-like non-polyhedral Pt nanoparticles with their diversity and variety of surface morphologies in the single-crystal nucleation and growth. In addition, Pt nanorod about 20 nm was also formed in Fig. 3(a) and (e). Two assumed models of sphere-like non-polyhedral and octahedral Pt nanoparticles were used to illustrate our experimental results. Especially, there were two corners of octahedral Pt nanoparticles that were truncated in the final morphology. The results showed that the atomic arrangement of HRTEM image of octahedral Pt nanoparticles is more stable than that of sphere-like Pt nanoparticles in Fig. 3(e–f).

3.3. Size and morphology of Pd nanoparticles and Pt–Pd core-shell nanoparticles

Fig. 4 shows the large Pt–Pd bimetallic nanoparticles of core-shell morphologies in the nanosized range of 20–25 nm based on the as-prepared and defined Pt cores (Sample 3). So far, the methods of controlling metal core-shell have been difficult because of the alloying of two different metals [24,28]. For a common phenomenon, the surface contacts between smaller Pd nanoparticles and bigger Pt–Pd nanoparticles were established. This led to form the irregular and large particles. Therefore, the large and irregular particles were formed by the surface attachments, self-aggregation and assembly in the case of removing PVP in Fig. 4(a and b). The Pd nanoparticles attached and deposited on the surfaces of larger particles, such as Pt–Pd core-shell nanoparticles. At the contacts at their interfaces, the re-crystallization occurred. In Fig. 4(b), the re-crystallization of nanoparticles needs to be considered. However, the re-crystallization of the layers between the core and the shell in Fig. 4(e), (f), and (h) were clearly shown in the epitaxial and non-epitaxial growth modes. Near-sphere Pd nanoparticle of 5–10 nm were observed. An HRTEM image of a single Pd nanoparticle (Fig. 4(g) showed the Pd lattice fringes with the inter-fringe distance d1 ~ 0.230 nm assigned to the distance between the {1 1 1} planes showing Pd crystal of face-centered cubic (fcc) structure. In this case, it is certain that the effect of the synthetic approach using the assistance of $AgNO_3$ to control the sharp and polyhedral morphology was not clearly determined from these Pd nanoparticles.

Based on the classical theory of nucleation and growth of single metal nanoparticles as well as the nucleation and growth of alloy

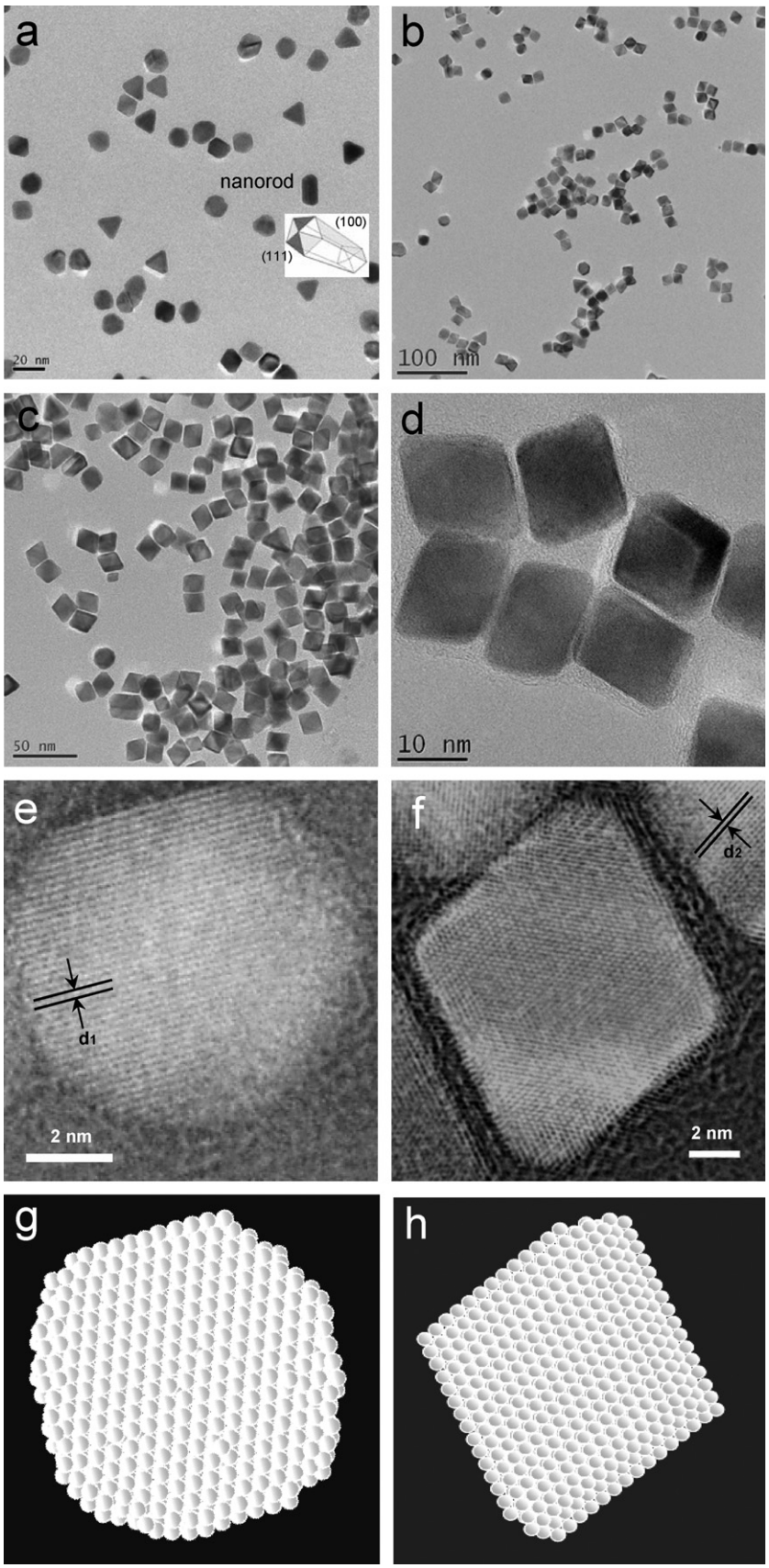

Fig. 3. TEM and HRTEM images of Pt nanoparticles: (a)–(e) unsharp, sharp and polyhedral; (b)–(d) and (f) sharp and polyhedral; (g)–(h) two assumed models of Pt nanoparticles are given.

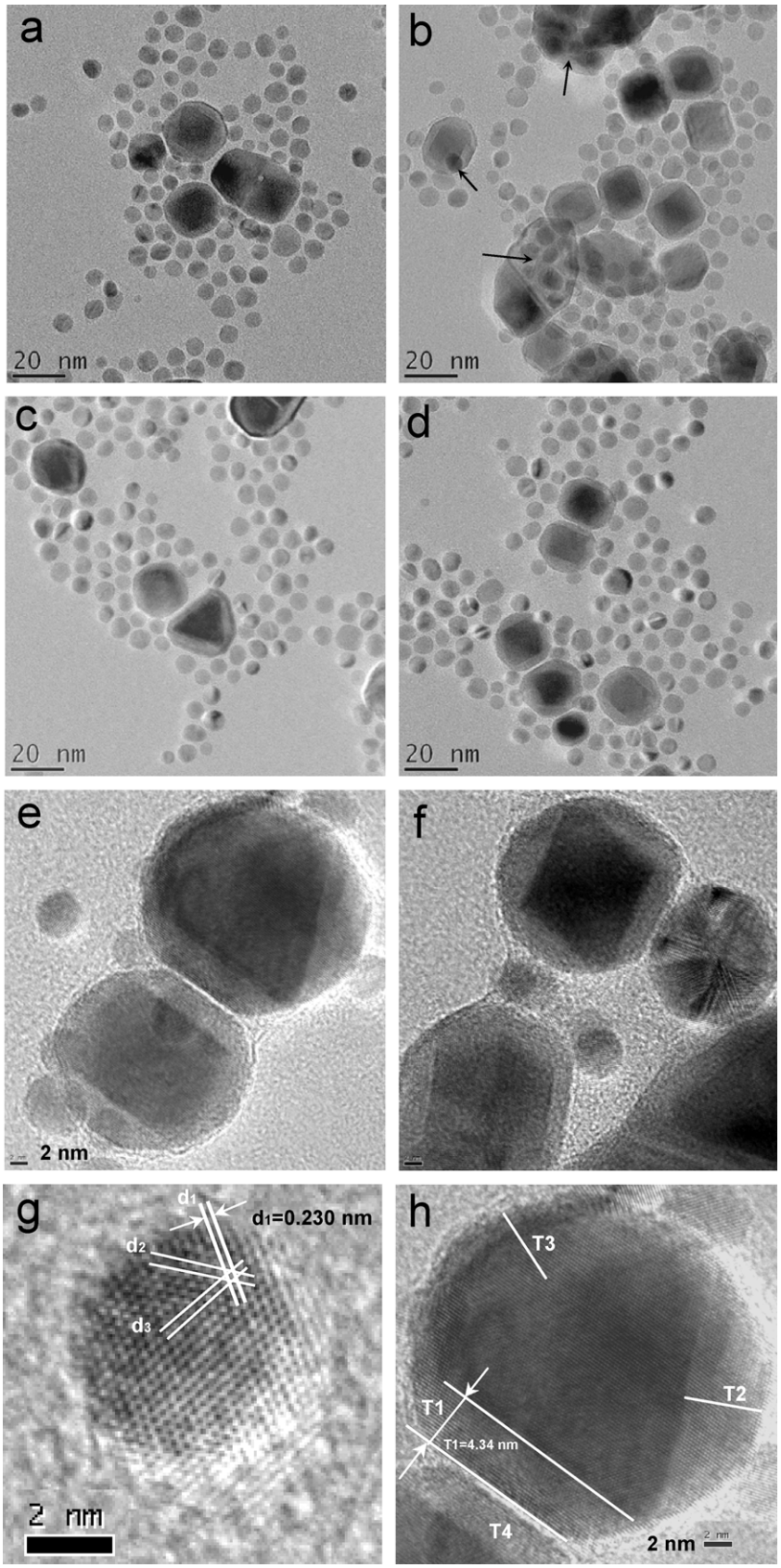

Fig. 4. (a)–(f) TEM and HRTEM of Pd nanoparticles and Pt–Pd core-shell nanoparticles. The formation of Pt–Pd core-shell nanoparticles from the as-prepared polyhedral Pt seeds. The Pt cores were protected by the Pd shells. (g) Pd nanoparticle ~6 nm. (h) Pt–Pd core-shell nanoparticle based on the tetrahedral Pt core. The layer-by-layer overgrowth (SK) was observed in the T1 and T4-shell layers. Scale bars: (a)–(d) 2 nm; (e)–(h) 2 nm.

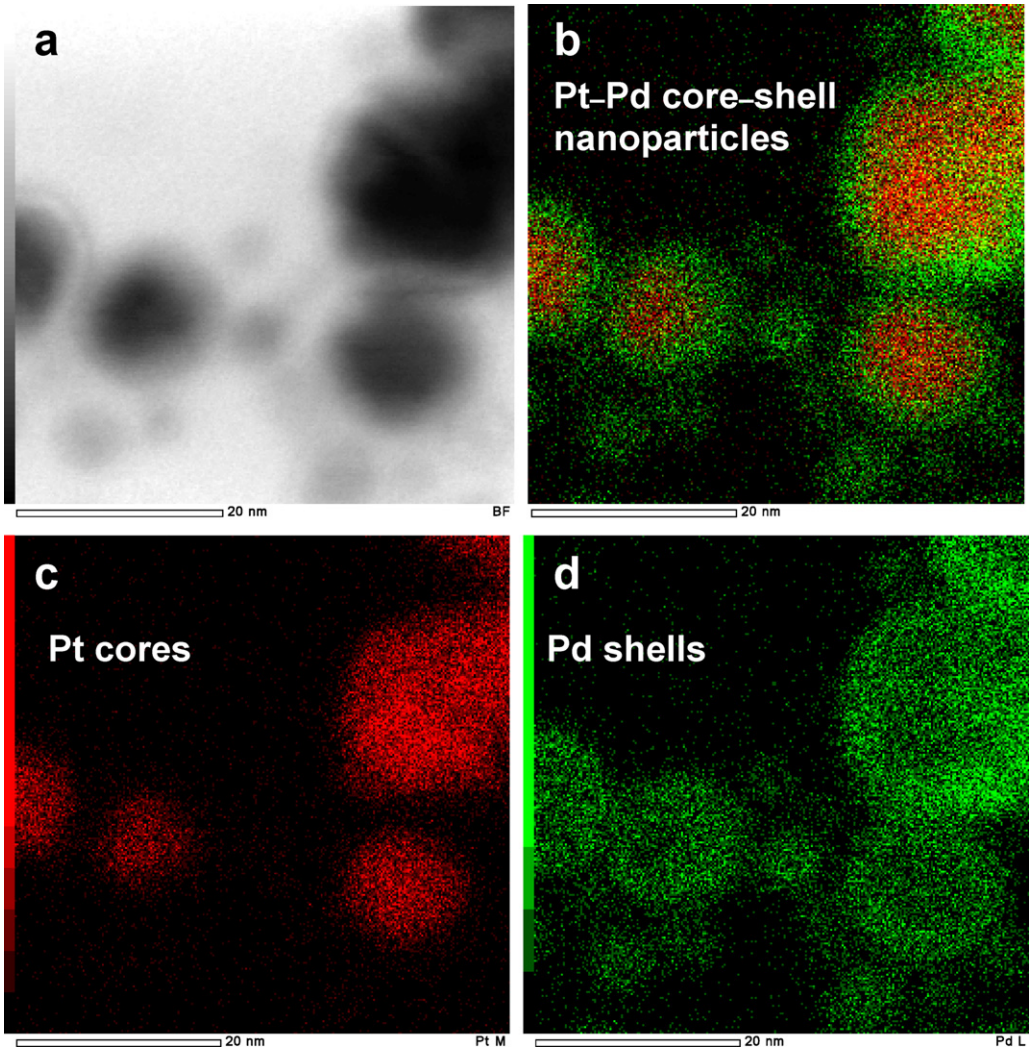

Fig. 5. HAADF-STEM image and STEM-XEDS elemental maps of Pt–Pd core-shell nanoparticles: (a) HAADF image. (b) Color overlay emphasizes of the spatial extent of each signal to Pd and Pt elements revealing the core-shell nature of Pt–Pd nanoparticles. (c) Pt Mα (red). (d) Pd Lα (green). Scale bars: 20 nm. (For interpretation of the references to color in this figure legend, the reader is referred to the web version of the article.)

and core-shell bimetal nanoparticles, the Gibbs free energy and overall excess free energy were considered in order to control their size and morphology for uniform formation of the core and/or the shell. In general, the Frank–van der Merwe (FM), Volmer–Weber (VW), and Stranski–Krastanov (SK) growth modes have explained the formation of various nanostructures of Pt–Pd based alloy, and Pt-based core-shell nanoparticles [3,4,34].

On the fundamental of the density functional theory (DFT) in surface chemistry and catalysis, Pt–Pd bimetal nanoparticles are considered as the great candidates in catalysis [36]. The main reasons are the high oxygen reduction activity of Pt and Pd metal catalysts because they are confirmed in their activity on the top of the volcano curve among transition metals according to the d-band theory, such as Ir, Cu, Ag... for obtaining the high ORR activity [36,37]. At present, Pt or Pd based nanocatalysts are increasingly developed because they are highly active electrocatalysts in fuel cells, especially for the commercialization and realization of direct methanol fuel cells (DMFC) [38–44]. Thus, Pt–Pd nanocatalysts become a suitable choice of replacing Pt–Ru nanocatalysts in DMFCs because the cost of Pt–Ru nanocatalysts is much higher [45–51]. Therefore, the feasible solutions of core-shell bimetallic nanoparticles with a thin Pt or Pd shell (as atomic monolayers) to reduce the Pt loadings are studied in the development of PEMs and DMFCs [52–54]. In addition, the lattice-strain control of the activity in dealloying the core-shell catalysts was studied in the Pt–Cu bimetallic nanoparticles. This characterization enables to reduce amount of Pt-nanocatalyst loading by more than 80% [55].

Fig. 4(a–f) and (h) shows the TEM and HRTEM images of the FM and SK growth mode of the Pt–Pd core-shell nanoparticles. We suggested that the condition of the FM growth mode depended on the smooth surface of as-prepared polyhedral Pt nanoparticles, such as (1 1 1) facets.

The Pd monolayers were described by the overgrowth from atomic monolayers according to the FM mode. In the HRTEM image of Fig. 4(h), two different growth modes were observed in the shell-layer formation of tetrahedral Pt–Pd core-shell nanoparticle. It was the oriented overgrowth of the single crystal Pd shell on the surface of the as-prepared Pt core that possessed a good lattice match. In addition, both Pt and Pd metals have the (fcc) crystal structure. Therefore, the Pd shell could grow epitaxially on the Pt core because of their same crystal structures. The thickness of the shell layer of 18 ± 1 Pd atomic monolayers was approximately 4.34 nm in size. The overgrowth of atomic Pd monolayers of the tetrahedral Pt–Pd nanoparticles about $T1 = 4.34$ nm were formed in the FM growth mode in Fig. 4(h). The results provided the experimental evidence of phase segregation between the core (the as-prepared Pt nanoparticles) and the shell (the Pd coating). The thickness of Pd atomic monolayers or Pt shells, such as $T1$, $T2$, and $T3$ was very

different from their surfaces. The Pd overgrowth on the sharp corners of the as-prepared tetrahedral Pd nanoparticle was not preferential. At the same time, the directions of the overgrowth of atomic Pd monolayers of Pt–Pd core-shell nanoparticle were formed in both the FM and SK growth modes in Fig. 4(e). It was noted that the attachments of small Pd nanoparticles were the common modes to form a larger particle. They could deposit on the surfaces of larger particles leading to their combination at their interfaces. This mechanism is possibly very good to make the core-shell structures in various ways of the very mild and slow reduction of metal ions for making the shell. It means that very small clusters and nanoclusters will gradually deposit on the surfaces of as-prepared cores in the epitaxial growth modes (or both epitaxial and non-epitaxial overgrowth of shell metal). The phenomenon of small Pd nanoparticles deposited on the surfaces of Pt and Pt–Pd nanoparticles need to be addressed in the further studies. Fig. 5 shows HAADF-STEM images and STEM-XEDS elemental maps of Pt–Pd bimetallic nanoparticles with their intense contrast between the Pt cores and the Pd shells. These important evidences determine the nature of the core-shell nanostructures of Pt–Pd nanoparticles in the variations of chemical composition at atomic scale. Each set of STEM-XEDS presented individual elemental maps for Pd Lα, Pt Mα, and a color overlay map of two elements as the presentation of core-shell nanoparticles. Therefore, both TEM and STEM measurements indicated the existence of single Pd nanoparticles. Interestingly, the structural changes of polyhedral Pt cores were not significantly identified. So far, the great efforts are made to realize core-shell bimetallic nanoparticles under size and morphology control. Expectedly, the various sizes of layers of the shells and the cores are precisely controlled by varying the composition, reaction time and temperature, various kinds of metal precursors, polymers or ligands, reductants, and controlling reagents. A comparison of Pt nanoparticles and Pt–Pt core-shell nanoparticles will be our next research direction and goal.

4. Conclusions

In this study, Pt–Pd core-shell nanoparticles were successfully synthesized by modified polyol method based on the as-prepared polyhedral Pt seeds under size and morphology control. Some evidences of the epitaxial overgrowth of the Pd shell on the Pt core due to the layer-by-layer mechanism were confirmed. In our results, we have suggested that the Pt–Pd core-shell nanoparticles were formed in both the Frank–van der Merwe (FM) layer-by-layer and Stranski–Krastanov (SK) island-on-wetting-layer growth modes. The Pt–Pd core-shell nanoparticles were observed in the FM and SK growth modes, respectively. However, the latter became a favorable growth mode in the formation of Pt–Pd core-shell nanoparticles.

Acknowledgements

We would like to thank Toyota Company and Dr Hirata for his helpfulness in our program of the research and development of science and nanotechnology in Japan.

References

[1] M.A. El-Sayed, Acc. Chem. Res. 34 (2001) 257–264.
[2] M. Subhramannia, V.K. Pillai, J. Mater. Chem. 18 (2008) 5858–5870.
[3] Z. Peng, H. Yang, Nano Today 4 (2009) 143–164.
[4] J Chen, B. Lim, E.P. Lee, Y. Xia, Nano Today 4 (2009) 81–95.
[5] M. Nakamura, Y. Hanioka, W. Ouchida, M. Yamada, N. Hoshi, Chem. Phys. Chem. 10 (2009) 2719–2724.
[6] K. Lee, M. Kim, H. Kim, J. Mater. Chem. 20 (2010) 3791–3798.
[7] L.C. Gontard, L.Y. Chang, C.J. Hetherington, A.I. Kirkland, D. Ozkaya, R.E. Dunin-Borkowski, Angew. Chem. Int. Ed. Engl. 46 (2007) 3683–3685.
[8] L.Y. Chang, A.S. Barnard, L.C. Gontard, R.E. Dunin-Borkowski, Nano Lett. 10 (2010) 3073–3076.
[9] P. Urchaga, S. Baranton, T.W. Napporn, C. Coutanceau, Electrocatalysis 1 (2010) 3–6.
[10] Y. Borodko, L. Jones, H. Lee, H. Frei, G. Somorjai, Langmuir 25 (2009) 6665–6671.
[11] M. Cabié, S. Giorgio, C.R. Henry, M.R. Axet, K. Philippot, B. Chaudret, J. Phys. Chem. C 114 (2010) 2160–2163.
[12] V. Mazumder, Y. Lee, S. Sun, Adv. Funct. Mater. 20 (2010) 1224–1231.
[13] H. Zhang, Y. Yin, Y. Hu, C. Li, P. Wu, S. Wei, C. Cai, J. Phys. Chem. C 114 (2010) 11861–11867.
[14] H. Lee, S.E. Habas, G.A. Somorjai, P. Yang, J. Am. Chem. Soc. 130 (2008) 5406–5407.
[15] N. Toshima, H. Yan, Y. Shiraishi, Recent progress in bimetallic nanoparticles: their preparation structures and functions, in: B. Corain, G. Schmid, N. Toshima (Eds.), Metal Nanoclusters in Catalysis and Materials Science: The Issue of Size Control, Elsevier B.V., 2004, pp. 49–75.
[16] Y. Wang, N. Toshima, J. Phys. Chem. B 101 (1997) 5301–5306.
[17] J. Yang, E. Sargent, S. Kelley, J.Y. Ying, Nat. Mater. 8 (2009) 683–689.
[18] P. Venkatesan, J. Santhanalakshmi, Langmuir 26 (2010) 12225–12229.
[19] F. Bernardi, M.C.M. Alves, A. Traverse, D.O. Silva, C.W. Scheeren, J. Dupont, J. Morais, J. Phys. Chem. C 113 (2009) 3909–3916.
[20] F. Bernardi, G.H. Fecher, M.C.M. Alves, J. Morais, J. Phys. Chem. Lett. 1 (2010) 912–917.
[21] J. Luo, L. Wang, D. Mott, P.N. Njoki, Y. Lin, T. He, Z. Xu, B.N. Wanjana, I.S. Lim, C. Zhong, Adv. Mater. 20 (2008) 4342–4347.
[22] T. Lopes, E. Antolini, E.R. Gonzaleza, Int. J. Hydrogen Energy 33 (2008) 5563–5570.
[23] U. Nilekar, S. Alayoglu, B. Eichhorn, M. Mavrikakis, J. Am. Chem. Soc. 132 (2010) 7418–7428.
[24] R. Ferrando, J. Jellinek, R.L. Johnston, Chem. Rev. 108 (2008) 845–910.
[25] Y. Xia, Y. Xiong, B. Lim, S.E. Skrabalak, Angew. Chem. Int. Ed. 48 (2009) 60–103.
[26] H. Goesmann, C. Feldmann, Angew. Chem. Int. Ed. 49 (2010) 1362–1395.
[27] S. Shylesh, V. Schünemann, W.R. Thiel, Angew. Chem. Int. Ed. 49 (2010) 3428–3459.
[28] L. Carbone, P.D. Cozzoli, Nano Today 5 (2010) 449–493.
[29] H. Song, F. Kim, S. Connor, G.A. Somorjai, P. Yang, J. Phys. Chem. B 109 (2005) 188–193.
[30] T. Teranishi, M. Hosoe, T. Tanaka, M. Miyake, J. Phys. Chem. B 103 (1999) 3813–3827.
[31] A.R. Tao, S. Hamas, P. Yang, Small 4 (2008) 310–325.
[32] H. Choo, B. He, K.Y. Liew, H. Liu, J. Lin, J. Mol. Catal. A 224 (2006) 217–228.
[33] H. Zhang, C. Wang, J. Wang, J. Zhai, W. Cai, J. Phys. Chem. C 114 (2010) 6446–6451.
[34] T. Sugimoto, Part 2: Preparation, in: T. Sugimoto (Ed.), Monodispersed Particles, Elsevier, Amsterdam, 2001, pp. 187–441.
[35] A. Chen, P. Holt-Hindle, Chem. Rev. 110 (2010) 3767–3804.
[36] J.K. Nørskov, J. Rossmeisl, A. Logadottir, L. Lindqvist, J. Kitchin, T. Bligaard, H. Jónsson:, J. Phys. Chem. B 108 (2004) 17887–17892.
[37] J.K. Nørskova, F. Abild-Pedersen, F. Studt, T. Bligaard, Density functional theory in surface chemistry and catalysis, 1006652108 (2011) 1–7, www.pnas.org/cgi/doi/10.1073/pnas.
[38] E. Antolini, Energy Environ. Sci. 2 (2009) 915–931.
[39] A. Gewirth, M.S. Thorum, Inorg. Chem. 49 (2010) 3557–3566.
[40] C. Bianchini, P.K. Shen, Chem. Rev. 109 (2009) 4183–4206.
[41] M.H. Seo, E.J. Lim, S.M. Choi, H.J. Kim, W.B. Kim, Top. Catal. 53 (2010) 678–685.
[42] Y. Shao-Horn, W.C. Sheng, S. Chen, P.J. Ferreira, E.F. Holby, D. Morgan, Top. Catal. 46 (2007) 285–305.
[43] R.R. Adzic, J. Zhang, K. Sasaki, M.B. Vukmirovic, M. Shao, J.X. Wang, A.U. Nilekar, M. Mavrikakis, J.A. Valerio, F. Uribe, Top. Catal. 46 (2007) 249–262.
[44] Y. Shao, J. Liu, Y. Wang, Y. Lin, J. Mater. Chem. 19 (2009) 46–59.
[45] Y. Cho, B. Choi, Y. Cho, H. Park, Y. Sung, Electrochem. Commun. 9 (2007) 378–381.
[46] A.M. Zainoodin, S.K. Kamarudin, W.R.W. Daud, Int. J. Hydrogen Energy 35 (2010) 4606–4621.
[47] S. Alayoglu, A.U. Nilekar, M. Mavrikakis, B. Eichhorn, Nat. Mater. 7 (2008) 333–338.
[48] E. Antolini, Mater. Chem. Phys. 78 (2003) 563–573.
[49] E. Antolini, J.R.C. Salgado, E.R. Gonzalez, J. Power Sources 160 (2006) 957–968.
[50] E. Antolini, Appl. Catal. B 74 (2007) 324–336.
[51] E. Antolini, Appl. Catal. B 74 (2007) 337–350.
[52] H. Yang, Angew. Chem. Int. Ed. 50 (2011) 2674–2676.
[53] N.V. Long, T. Asaka, T. Matsubara, M. Nogami, Acta Mater. 59 (2011) 2901–2907.
[54] J. Butler, S. Coles, M. Ryan, K. White, Platinum Metal Rev. 55 (2011) 1–72.
[55] P. Strasser, S. Koh, T. Anniyev, J. Greeley, K. More, C. Yu, Z. Liu, S. Kaya, D. Nordlund, H. Ogasawara, M.F. Toney, A. Nilsson, Nat. Chem. 2 (2010) 454–460.